available at www.sciencedirect.com

ScienceDirect

journal homepage: www.elsevier.com/locate/biochempharm

The mechanism causing the difference in kinetic properties between rat CYP2D4 and human CYP2D6 in the oxidation of dextromethorphan and bufuralol

Shizuo Narimatsu [a,*], *Daichi Kazamori* [a], *Kazufumi Masuda* [b], *Takashi Katsu* [a], *Yoshihiko Funae* [c], *Shinsaku Naito* [d], *Hironori Nakura* [a], *Shigeru Yamano* [e], *Nobumitsu Hanioka* [a]

[a] *Graduate School of Medicine, Dentistry and Pharmaceutical Sciences, Okayama University, 1-1-1 Tsushima-naka, Okayama 700-8530, Japan*
[b] *School of Pharmacy, Shujitsu University, 1-6-1 Nishigawara, Okayama 700-8516, Japan*
[c] *Osaka City University Medical School, 1-4-54 Asashi-machi, Abeno-ku, Osaka 548-8585, Japan*
[d] *Research and Development Center, Otsuka Pharmaceutical Factory Inc., Naruto, Tokushima 772-8601, Japan*
[e] *Faculty of Pharmaceutical Sciences, Fukuoka University, 8-19-1 Nanakuma, Minami-ku, Fukuoka 810-0180, Japan*

ARTICLE INFO

Article history:
Received 25 September 2008
Accepted 6 November 2008

Keywords:
CYP2D4
CYP2D6
Bufuralol
Dextromethorphan
Nonlinear kinetics
Site-directed mutagenesis

ABSTRACT

The capacity to oxidize bufuralol (BF) and dextromethorphan (DEX) was compared kinetically between human CYP2D6 and four rat CYP2D (CYP2D1, -2D2, -2D3 and -2D4) isoenzymes in a yeast cell expression system. In BF 1″-hydroxylation and DEX O-demethylation, only CYP2D4 showed hook-shaped Eadie–Hofstee plots, the other four CYP2D enzymes exhibiting linear plots. In DEX N-demethylation, rat CYP2D2 did not show any detectable activity under the conditions used, whereas the other four enzymes yielded linear Eadie–Hofstee plots. To elucidate the mechanisms causing the nonlinear kinetics, four CYP2D4 mutants, CYP2D4-F109I, -V123F, -L216F and -A486F, were prepared. CYP2D4-V123F, -L216F and -A486F yielded linear or linear-like Eadie–Hofstee plots for BF 1″-hydroxylation, whereas only CYP2D4-A486F exhibited linear plots for DEX O-demethylation. The substitution of Phe-109 by isoleucine did not have any effect on the oxidative capacity of CYP2D4 for either BF or DEX. These results suggest that the introduction of phenylalanine in the active-site cavity of CYP2D4 simplifies complicated interactions between the substrates and the amino acid residues, but the mechanisms causing the simplification differ between BF and DEX.

1. Introduction

Cytochrome P450 2D6 (CYP2D6) is an important CYP enzyme involved in drug metabolism in the human liver. CYP2D6 is a major oxidative isoenzyme, affecting the metabolic fate of about 30% of medicines that are often prescribed clinically [1,2], although its level in the human liver is relatively low (about 2% of total CYP content) [1,3]. Furthermore, CYP2D6 shows extensive genetic polymorphism, promoting the concept of tailor-made chemotherapy [4,5]. It is therefore essential in the development of new medicines or performing efficient tailor-made chemotherapy to sufficiently understand the properties of the wild-type CYP2D6 protein and its variants.

Studying the influence of the substitution of an amino acid residue caused by a single nucleotide polymorphism can reveal the role of the residue, which may elucidate the mechanism behind the enzymatic reaction. A

* *Corresponding author*. Tel.: +81 86 251 7942; fax: +81 86 251 7942.
E-mail address: shizuo@pharm.okayama-u.ac.jp (S. Narimatsu).
0006-2952/$ – see front matter
doi:10.1016/j.bcp.2008.11.006

comparative study of the structural biochemistry and enzymology of orthologous enzymes between different animal species is also useful for understanding enzymatic functions [6].

The rat is used extensively in biological, pharmacological and toxicological research. It is recognized that four functional CYP2D isoenzymes, CYP2D1, -2D2, -2D3 and -2D4, are expressed in various rat organs and tissues, particularly, CYP2D4 is expressed in various regions of the rat brain [7]. This isoenzyme may therefore have some physiological roles in the rat brain [8,9].

Among the four rat CYP2D enzymes, the substrate specificity of CYP2D2 is most similar to that of human CYP2D6 in various experiments using typical substrates such as debrisoquine, bufuralol, propranolol and so on [7,10–12]. In the oxidation of these substrates in the active-site cavity of CYP2D6, several amino acid residues such as Phe-120 [13–15], Glu-216 [15–17], Asp-301 [15,18] and Phe-483 [15] have been proposed to be involved in capturing the substrate via ionic or hydrophobic interaction. By analogy to the substrate specificity for CYP2D6, we speculate that Glu-219 and Asp-304, corresponding to Glu-216 and Asp-301 of human CYP2D6, respectively, have similar roles in the interaction in the active-site cavity of rat CYP2D2. As compared with human CYP2D6, little information is available on the interaction between substrates and amino acid residues in the active-site cavity of rat CYP2D enzymes. As described above, the rat is useful in both in vivo and in vitro studies in the research fields of drug-development, metabolism and toxicity. Therefore, further understanding of the properties of rat CYP2D enzymes and differences between rat and human CYP2D enzymes is necessary not only for elucidation of molecular mechanisms involved in various CYP2D enzyme-catalyzed reactions but also for the early stages of drug-development using the rat.

In this research using a yeast cell expression system to further characterize rat CYP2D4, enzymatic properties were compared with those of human CYP2D6, by focusing on the functions of certain amino acid residues, all of which are located in the substrate recognition sites (SRSs) [19].

2. Materials and methods

2.1. Materials

Racemic bufuralol (BF) and its 1″-hydroxybufuralol (1″-OH-BF as hydrochloride) were obtained from Ultrafine Chemicals (Manchester, UK). Dextromethorphan (DEX), dextrorphan (DXO) and 3-methoxymorphinan (MEM) were purchased from Sigma–Aldrich (St. Louis, MO). Glucose 6-phosphate (G-6-P) and G-6-P dehydrogenase and NADPH were purchased from Oriental Yeast Co. (Tokyo, Japan). The QuikChange site-directed mutagenesis kit was obtained from Stratagene (La Jolla, CA); the polyvinylidene difluoride (PVDF) membrane was from Millipore (Billerica, MA). A polyclonal antibody (antiserum) raised against human CYP2D6 was obtained by immunizing adult male white Japanese rabbits with a mixture of complete Freund adjuvant and purified CYP2D6 in this laboratory. All other chemicals and reagents used were of the highest quality commercially available.

Table 1 – Primers used for side-directed mutagenesis for CYP2D4 cDNA.

Primer	Mutation	Sequence
F109I-F	325T > A	GGCCACCGCTGCATATCAAT-GACCAGTCGG
F109I-R		CCGACTGGTCATTGATATG-CAGCGGTGGCC
V123F-F	367G > T	CGCTCTCAAGGTGTGTTCCTCGC-GAGGTATGG
V123F-R		CCATACCTCGCGAGGAACA-CACCTTGAGAGCG
L216F-F	646C > T	GCACTTGCTGAAGGACACTTTT-GAGGAGGAATCTG
L216F-R		CAGATTCCTCCT-CAAAAGTGTCCTTCAGCAAGTCC
A486F-F	1456G > T	GGCGTCTTTGGTTTTCTGAC-CACCCCGCGC
A486F-R	1457C > T	GCGCGGGGTGGTCAGAAAAC-CAAAGACGCC

Underlines indicate the mutations introduced by PCR-based mutagenesis.

2.2. Construction of plasmids and expression in yeast cells

The construction of plasmids and the expression in yeast cells of rat CYP2D1 and CYP2D2 [6] and human CYP2D6 [20] were performed according to the methods described previously. CYP2D3 and CYP2D4 cDNAs with HindIII sites at the 5′- and 3′-ends cloned into pBluescript-SK(±) (pBluescript/CYP2D3 and pBluescript/CYP2D4) were provided by Dr. Funae (Osaka City University) [21]. Each of the plasmids contains a Kozak sequence upstream of the start codon to achieve a high level of expression of protein in yeast cells. Four mutant cDNAs (CYP2D4-F109I, -V123F, -L216F and -A486F) were prepared from CYP2D4 cDNA with the QuikChange site-directed mutagenesis kit as described previously [22]. The sets of forward and reverse primers are listed in Table 1. To ensure that no errors had been introduced during the amplification process, the plasmids were verified by DNA sequencing. Yeast cells (*Saccharomyces cerevisiae* AH-22) were then transfected with pGYRI containing each of the mutated CYP2D4 cDNAs to express the corresponding mutated rat CYP2D proteins [6,21,23].

2.3. Assay of CYP2D proteins

Yeast cell microsomal fractions were prepared by a previously published method [23]. Total CYP content was measured immunochemically as follows. Appropriate portions of yeast cell microsomal fractions were subjected to sodium dodecyl sulfate-polyacrylamide gel electrophoresis (SDS-PAGE) using a 10% slab gel. Proteins in the gel were electroblotted to a PVDF membrane, and analyzed by Western blotting [24] using rabbit antiserum raised against human CYP2D6. Total holo-CYP content was measured spectrophotometrically by the method of Omura and Sato [25] using 91 mM^{-1} cm^{-1} as an absorption coefficient.

2.4. Assay of drug-oxidizing activities

Racemic BF 1″-hydroxylase activities were determined by high-performance liquid chromatography (HPLC) according to a published method [26]. Briefly, a typical reaction mixture consisted of 10 mM $MgCl_2$, 0.2 mM EDTA 2Na, 10 mM G-6-P, 0.2 U G-6-P dehydrogenase, 1 mM NADPH, 1–200 μM BF, 5.0 mg protein/mL recombinant CYP2D enzyme and 50 mM potassium phosphate buffer (pH 7.4) in a final volume of 400 μL. BF was dissolved in a mixture of dimethylsulfoxide/methanol (50:50 by volume), and the final concentration of the organic solvent was 1%. Following preincubation at 37 °C for 1 min, incubation was started by adding the microsomal fraction, continued for 10 min and terminated by adding aqueous 2 M phosphoric acid and vigorous shaking. The mixture was centrifuged at 14,000 × *g* for 10 min at 4 °C and the supernatant was passed through a polytetrafluoroethylene membrane filter (pore size of 0.45 μm, Millipore). A portion (50 μL) of the filtrate was subjected to HPLC under the conditions as follows: HPLC apparatus, DP-8020 pump, AS-8021 autosampler, CO-8020 column oven, LC-8020 v 1.3 software data processor (Toso, Tokyo, Japan), L-7485 fluorescence detector (Hitachi, Tokyo, Japan); column, Inertsil ODS-80A (particle size 5 μm, 4.6 mm i.d. × 150 mm, GL Sciences, Tokyo, Japan); column temperature, 40 °C; mobile phase, 20 mM sodium perchlorate (pH 2.5)/acetonitrile/methanol (68:16:16, by volume); flow rate, 1.2 mL/min: detection, fluorescence (excitation/emission wavelength, 252/297 nm); injection volume, 50 μL. The amount of 1″-OH-BF was calculated on the basis of calibration curves made by spiking known amounts of the synthetic metabolite into the reaction mixture without the incubation.

DEX *O*- and *N*-demethylase activities were measured by the method of Kronbach et al. [27] with a slight modification. Briefly, half-scale reaction mixture as described for BF oxidation contained 10.0 mg protein/mL of recombinant CYP2D enzyme and 2–500 μM DEX. DEX was dissolved in aqueous 50% methanol, and the final concentration of the organic solvent was 1%. The following manipulation, except for the incubation period of 5 min, was the same as for the BF oxidation assay. A portion (20 μL) of the filtrate was subjected to HPLC under conditions as follows: HPLC apparatus, L-2130 pump, L-2300 column oven, L-2480 fluorescence detector and D-2000 v. 1.1 software data processor (Hitachi, Tokyo, Japan); column, Inertsil Ph-3 (particle size 5 μm, 4.6 mm i.d. × 150 mm, GL Sciences); column temperature, 40 °C; mobile phase, 20 mM potassium dihydrogen phosphate (pH 3.5)/acetonitrile (75:25, by volume); flow rate, 1.0 mL/min: detection, fluorescence (excitation/emission wavelength, 280/310 nm); injection volume, 20 μL. The amounts of DXO and MEM were calculated on the basis of calibration curves made by spiking known amounts of the synthetic metabolites into the reaction mixture without the incubation. Enzyme assays and kinetic analyses were performed three times with different lots of recombinant enzymes and carried out in duplicate. Enzyme kinetics were analyzed with Michaelis–Menten plots, Eadie–Hofstee plots and Hill plots using Prism v. 4.0 (GraphPad Software, San Diego, CA) and SigmaPlot v. 8.0 (Systat Software, San Jose, CA). Kinetic parameters were expressed as the mean ± S.D. ($n = 3$), and statistical significance was calculated with Dunnett's *post hoc* test. A probability of $p < 0.05$ was considered significant.

2.5. Molecular modeling

The conformation of CYP2D4 was automatically constructed by Swiss-Model (http://swissmodel.exspacy.org/SWISS-MODEL.html) using the crystallographic data of CYP2D6 (2F9Q) obtained from Protein Data Bank (http://www.rcsb.org/pbd/). Six peptides (104–126, 209–220, 244–249, 300–314, 370–379, and 480–488) were extracted as SRSs [19], and energy optimization was performed using Insight II/Discover as described previously [13]. The conformations of CYP2D4 and its mutants were drawn using RasMol v. 2.6-ucb-1.0.

3. Results

3.1. Expression of human CYP2D6 and rat CYP2D1, -2D2, -2D3 and -2D4 proteins in yeast cell microsomes

Microsomal fractions (10 μg of microsomal protein each) from yeast cells expressing each of the human and rat CYP2D isoenzymes were subjected to SDS-PAGE, and analyzed by Western blotting. As shown in Fig. 1A, protein bands that cross-reacted with the polyclonal antibody raised against human CYP2D6 were observed for all of the yeast cell

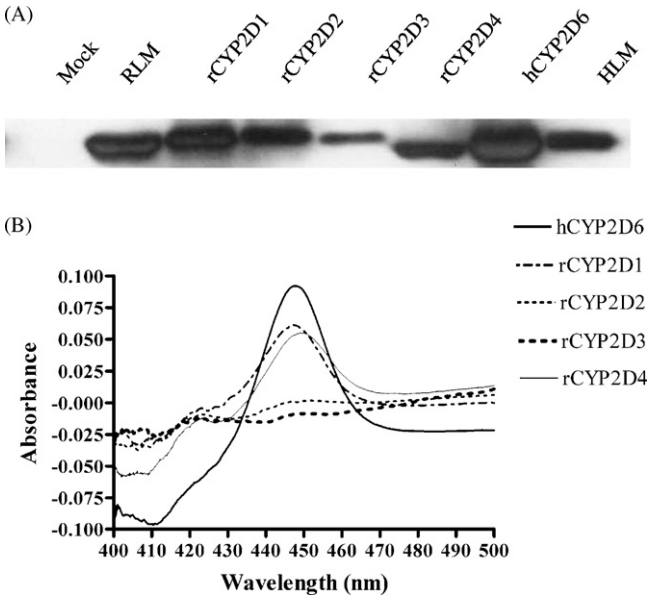

Fig. 1 – Western blot analysis (A) and reduced CO-difference spectra (B) of recombinant rat and human CYP2D enzymes in yeast cell microsomal fractions. (A) The amount of microsomal protein applied was 10 μg/lane. The CYP2D enzymes were probed with a rabbit polyclonal CYP2D6 antibody. RLM, rat liver microsomes (from adult male Sprague–Dawley rat); HLM, human liver microsomes (pooled sample obtained from BD Biosciences); hCYP, human CYP; rCYP, rat CYP. (B) The microsomal protein concentration was 10 mg/mL.

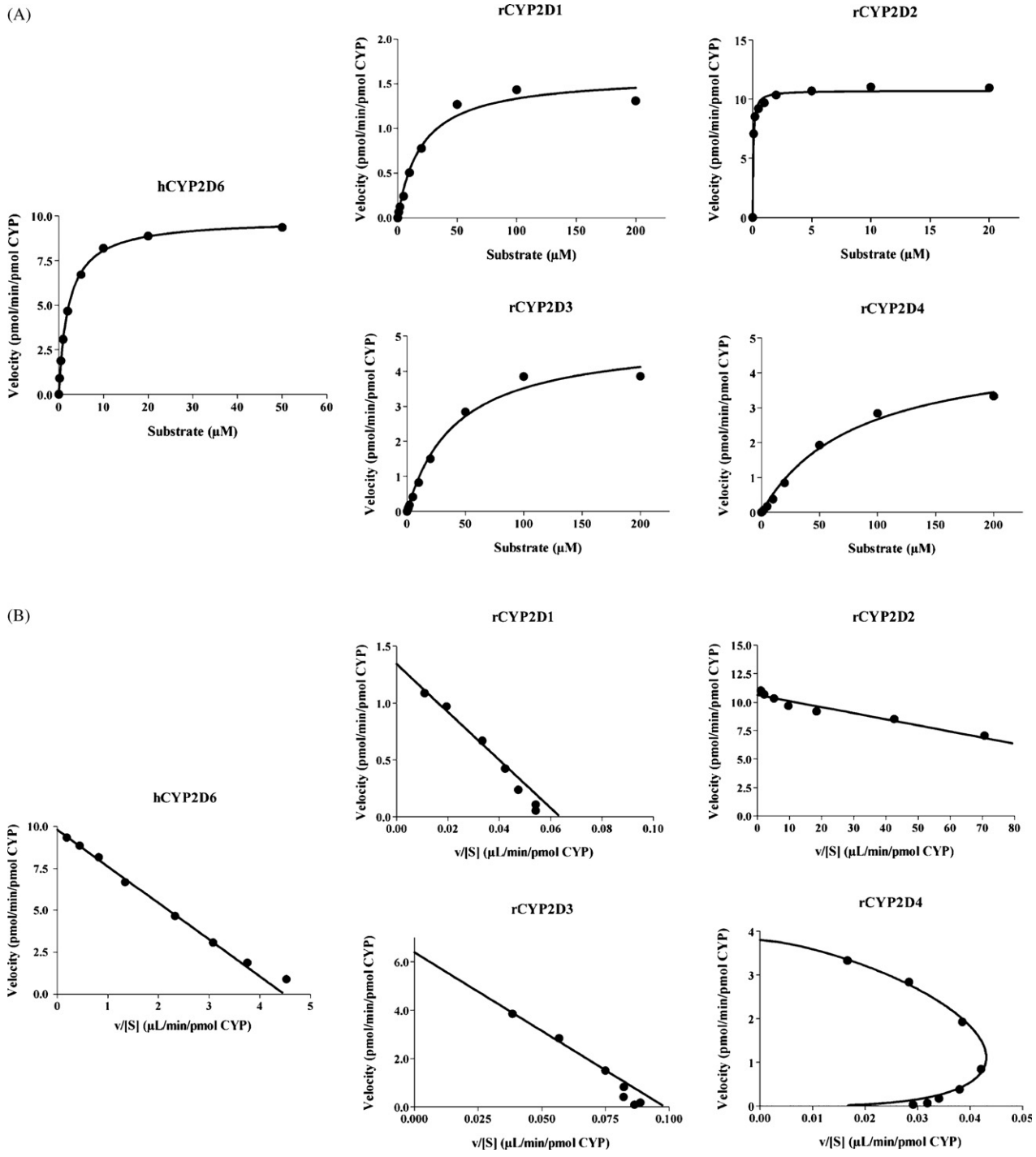

Fig. 2 – Michaelis–Menten plots (A) and Eadie–Hofstee plots (B) for BF 1″-hydroxylation by recombinant human CYP2D6 and four rat CYP2D enzymes. The substrate concentrations used were 0.2–50 μM for human CYP2D6, 1–200 μM for rat CYP2D1, -2D2 and -2D4, and 0.1–20 μM for rat CYP2D2. hCYP, human CYP; rCYP, rat CYP. Typical plots from three determinations are shown.

microsomal fractions except for mock. Staining intensity was high for CYP2D1 and CYP2D6, moderate for CYP2D2 and CYP2D4, and low for CYP2D3. Fig. 1B shows reduced CO-difference spectra of the recombinant CYP2D enzymes. Rat CYP2D1 and CYP2D4 as well as human CYP2D6 yielded typical spectra having a Soret peak at 450 nm, whereas CYP2D2 and CYP2D3 gave only a small peak at 450 nm. The contents calculated on the basis of the reduced CO-difference spectroscopy were 83.6 ± 15.5, 70.9 ± 9.8, 4.2 ± 2.2, 3.6 ± 0.7 and 47.3 ± 7.3 pmol/mg protein (the mean ± S.D. of three-independent expression samples), for CYP2D6, CYP2D1, CYP2D2, CYP2D3 and CYP2D4, respectively.

Table 2 – Kinetic parameters for BF 1″-hydroxylation by microsomes from yeast cells expressing human and rat CYP2D isoenzymes.

	K_m or S_{50}[a]	V_{max}[b]	n[c]	CL_{int} or CL_{max}[d]
hCYP2D6[e]	2.15 ± 0.41	14.1 ± 7.96		6.33 ± 2.48
rCYP2D1[e]	20.9 ± 0.86**	1.17 ± 0.54		0.06 ± 0.03
rCYP2D2[e]	0.50 ± 0.74	13.1 ± 10.0		86.0 ± 93.8
rCYP2D3[e]	37.6 ± 3.66**	6.42 ± 3.61		0.18 ± 0.11
rCYP2D4[f]	49.2 ± 1.03**	3.69 ± 1.10	1.39 ± 0.03	0.04 ± 0.01

Each value represents the mean ± S.D. for three separate experiments with independent preparations. hCYP, human CYP; rCYP, rat CYP.
[a] μM.
[b] pmol/min/pmol CYP.
[c] Hill coefficient.
[d] μL/min/pmol CYP.
[e] K_m, V_{max} and CL_{int} values were calculated by nonlinear regression to the Michaelis–Menten equation.
[f] S_{50}, V_{max} and CL_{max} values were calculated with the Hill equation.
** Significantly different from hCYP2D6 ($p < 0.01$).

3.2. *Kinetic analysis of BF 1″-hydroxylation by recombinant human and rat CYP2D enzymes*

Racemic BF 1″-hydroxylation by recombinant CYP2D enzymes was analyzed using Michaelis–Menten plots (Fig. 2A) and Eadie–Hofstee plots (Fig. 2B). It is of note that the Michaelis–Menten plots for BF oxidation by CYP2D4 exhibited a sigmoidal curve whereas the other four recombinant enzymes gave typical Michaelis–Menten plots (Fig. 2A). In Eadie–Hofstee plots (Fig. 2B), only CYP2D4 yielded a hook-shaped curve, while the other four enzymes gave lines. Kinetic parameters calculated are summarized in Table 2. Apparent K_m or S_{50} values were significantly higher for rat CYP2D1, CYP2D3 and CYP2D4 than for human CYP2D6, whereas the K_m values for rat CYP2D2 and human CYP2D6 were similar. The Hill coefficient for rat CYP2D4 was 1.4, indicating that the substrate might interact with multiple sites.

3.3. *Kinetic analysis of DEX oxidation by recombinant human and rat CYP2D isoenzymes*

The *O*- and *N*-demethylation of DEX by recombinant CYP2D enzymes was analyzed using Michaelis–Menten plots (Fig. 3A) and Eadie–Hofstee plots (Fig. 3B and C). As shown in the Michaelis–Menten plots (Fig. 3A), *O*-demethylation (closed circles) was preferred over *N*-demethylation (open circles) for human CYP2D6, rat CYP2D2 and CYP2D3. In contrast, *N*-demethylation predominated for rat CYP2D1 and CYP2D4. It should be noted that only the Eadie–Hofstee plots (Fig. 3B) for *O*-demethylation by rat CYP2D4 yielded a hook-shaped curve, whereas the plots for *O*- or *N*-demethylation by all of the recombinant enzymes, except for rat CYP2D2 showing no DEX *N*-demethylase activity, were linear. Kinetic parameters calculated are listed in Table 3. For *O*-demethylation, apparent K_m and S_{50} values were significantly higher for rat CYP2D1 and CYP2D4 than for human CYP2D6, whereas the V_{max} value for rat CYP2D3 was 3.5 times that for human CYP2D6. For *N*-demethylation, K_m and V_{max} values were significantly higher for CYP2D1 than for CYP2D6, while the V_{max} value for CYP2D4 was about 20-fold that for the human enzyme.

3.4. *Expression of rat CYP2D4 mutant proteins in yeast cell microsomes*

Among the four recombinant CYP2D enzymes, CYP2D4 showed hook-shaped Eadie–Hofstee plots both for BF 1″-hydroxylation and for DEX *O*-demethylation, but not for DEX *N*-demethylation. The hook-shaped kinetics indicate that the substrates may interact in a complicated manner with amino acid residues in the active-site cavity. We thus carefully looked at the amino acid residues in the six SRSs that can interact with BF and DEX in the active-site cavities of the five recombinant CYP2D isoenzymes (Fig. 4). Finally, we chose positions 109, 123 (within SRS-1), 216 (within SRS-2) and 486 (within SRS-6) of CYP2D4 as targets for the substitution of amino acid residues, because at least one of the recombinant CYP2D enzymes examined has a phenylalanine residue that can hydrophobically interact with the aromatic ring of the substrates.

We thus prepared plasmids encoding CYP2D4 mutants (CYP2D4-F109I, -V123F, -L216F and -A486F) and transformed yeast cells. Reduced CO-difference spectroscopy revealed that yeast cell microsomal contents of the four CYP2D4 mutants were at levels similar to that of the wild-type CYP2D4 (data not shown). The contents calculated on the basis of the spectroscopy were 47.3 ± 7.3, 80.4 ± 21.7, 50.0 ± 3.3, 60.9 ± 4.8 and 61.5 ± 2.2 pmol/mg protein (the mean ± S.D. of three-independent expression samples), for wild-type CYP2D4, CYP2D4-F109I, -V123F, -L216F and -A486F, respectively.

3.5. *Kinetic analysis of DEX oxidation by CYP2D4 mutants*

Fig. 5 shows Eadie–Hofstee plots for BF 1″-hydroxylation by wild-type CYP2D4 and its four mutants. Interestingly, CYP2D4-V123F and CYP2D4-A486F yielded linear plots, whereas CYP2D4-F109I as well as the wild-type enzyme gave hook-shaped kinetics. CYP2D4-L216F also exhibited a hook-shaped Eadie–Hofstee plots, however, the curve has a considerable linearity as compared with that for the wild-type CYP2D4. The kinetic parameters calculated are listed in Table 4. Apparent K_m (for CYP2D4-V123F) and S_{50} (for CYP2D4-L216F) values were significantly higher than the value for the

wild-type enzyme. Among the four mutants, only CYP2D4-L216F exhibited a significantly higher V_{max} value as compared with the wild-type CYP2D4. The Hill coefficient of CYP2D4-L216F was close to 1, indicating that the substitution of Leu-216 with phenylalanine tends to simplify the interaction of BF with amino acid residue(s) in the active-site.

Eadie–Hofstee plots for the oxidation of DEX by wild-type CYP2D4 and its mutants are shown in Fig. 6. DEX *O*-demethylation by wild-type CYP2D4 and three mutants gave hook-shaped plots, whereas only CYP2D4-A486F exhibited linear plots. In the case of *N*-demethylation, all of the mutants as well as the wild-type enzyme yielded linear Eadie–Hofstee

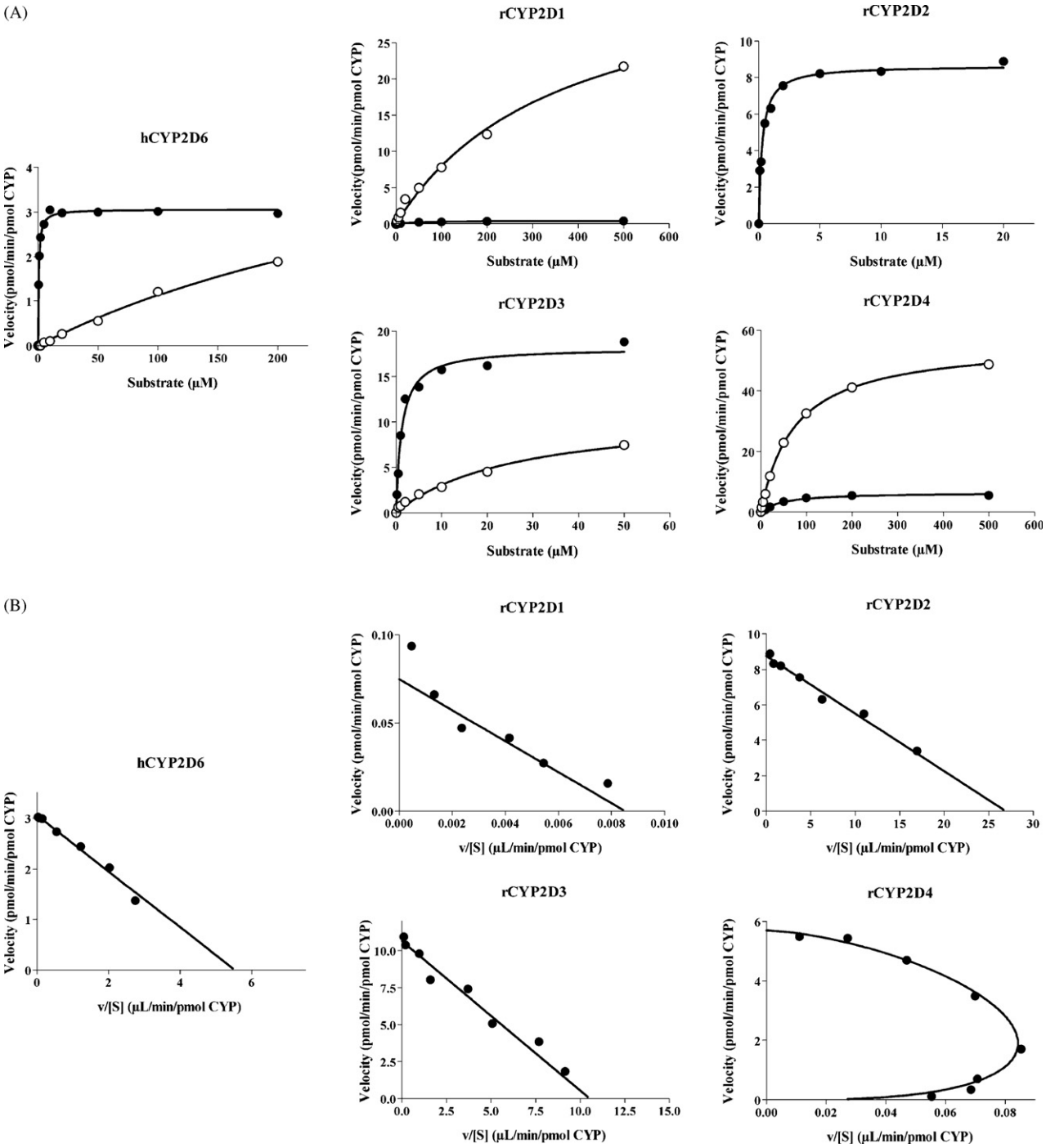

Fig. 3 – Michaelis–Menten plots for DEX oxidation (A) and Eadie–Hofstee plots for DEX *O*-demethylation (B) and *N*-demethylation (C) by recombinant human CYP2D6 and four rat CYP2D enzymes. The substrate concentrations used were 0.5–200 μM for human CYP2D6, 2–500 μM for rat CYP2D1 and -2D4, 0.1–20 μM for rat CYP2D2, and 0.2–50 μM for rat CYP2D3. hCYP, human CYP; rCYP, rat CYP. In Michaelis–Menten plots (A), closed circles, *O*-demethylation; open circles, *N*-demethylation. Typical plots from three determinations are shown.

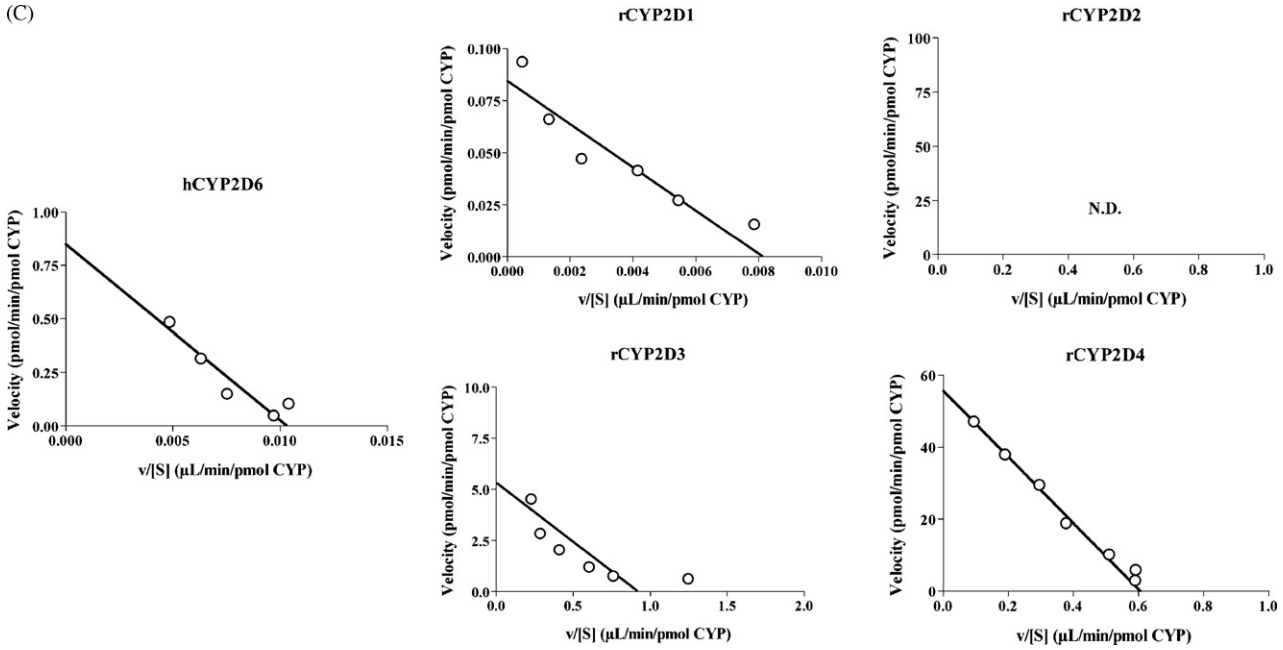

Fig. 3. (Continued).

plots. Kinetic parameters are listed in Table 5. For DEX *O*-demethylation, the S_{50} value of CYP2D4-A486F was significantly lower than the K_m value of the wild-type CYP2D4, whereas the V_{max} values were similar between the mutant and the wild-type enzyme. On the basis of clearance values (CL_{int} or CL_{max}), wild-type CYP2D4 as well as the three mutants (CYP2D4-F109I, -V123F and -L216F) preferred DEX *N*-demethylation over *O*-demethylation, while CYP2D4-A486F evenly mediated both *O*-demethylation and *N*-demethylation.

4. Discussion

In the present study, we compared the profiles of oxidation of BF and DEX between human CYP2D6 and four rat CYP2D isoenzymes (CYP2D1, -2D2, -2D3 and -2D4) using Michaelis–Menten plots and Eadie–Hofstee plots. We found that CYP2D4 exhibited hook-shaped Eadie–Hofstee plots for BF 1″-hydroxylation and DEX *O*-demethylation but linear plots for DEX *N*-demethylation, whereas the other rat CYP2D isoenzymes as

Table 3 – Kinetic parameters for DEX oxidation by microsomes from yeast cells expressing human and rat CYP2D isoenzymes.

CYP2D enzyme	K_m or S_{50}[a]	V_{max}[b]	n[c]	CL_{int} or CL_{max}[d]
O-Demethylation				
hCYP2D6[e]	1.28 ± 1.12	4.33 ± 1.88		4.32 ± 1.62
rCYP2D1[e]	49.0 ± 18.2**	0.13 ± 0.06		0.003 ± 0.002
rCYP2D2[e]	0.32 ± 0.19	6.45 ± 3.16		21.0 ± 8.34*
rCYP2D3[e]	0.96 ± 0.40	15.2 ± 3.67**		19.1 ± 12.3
rCYP2D4[f]	43.2 ± 7.56**	6.30 ± 1.36	1.43 ± 0.06	0.08 ± 0.009
N-Demethylation				
hCYP2D6[e]	235 ± 180	2.84 ± 2.84		0.010 ± 0.003
rCYP2D1[e]	638 ± 153**	44.3 ± 20.2**		0.08 ± 0.05
rCYP2D2[e]	N.D.	N.D.		N.D.
rCYP2D3[e]	44.2 ± 17.4	12.1 ± 1.42		0.30 ± 0.12
rCYP2D4[e]	94.6 ± 22.1	55.6 ± 0.65**		0.61 ± 0.15**

N.D., not detectable. Each value represents the mean ± S.D. for three separate experiments with independent preparations. hCYP, human CYP; rCYP, rat CYP.

[a] μM.

[b] pmol/min/pmol CYP.

[c] Hill coefficient.

[d] μL/min/pmol CYP.

[e] K_m, V_{max} and CL_{int} values were calculated by nonlinear regression to the Michaelis–Menten equation.

[f] S_{50}, V_{max} and CL_{max} values were calculated with the Hill equation.

* Significantly different from hCYP2D6 ($p < 0.05$).

** Significantly different from hCYP2D6 ($p < 0.01$).

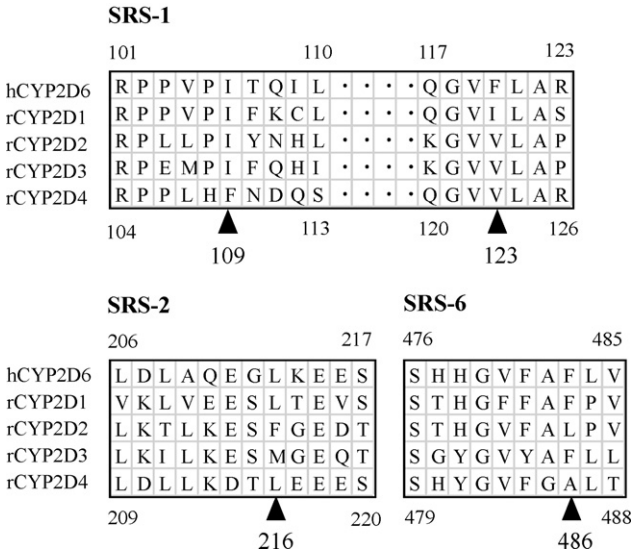

Fig. 4 – Alignment of partial amino acid sequences of human CYP2D6 and four rat CYP2D enzymes. The number at the top is for the human enzyme; the number at the bottom is for the rat enzymes. An arrowhead shows the amino acid residue to be substituted.

well as human CYP2D6 giving linear Eadie–Hofstee plots for all three metabolic reactions.

It is suggested from its crystal structure that CYP3A4 has a large active-site cavity to accommodate various small and large ligands, causing non-Michaelis–Menten kinetics [28]. However, it is unlikely that rat CYP2D4 has such a large active-site cavity because of the homology (78.0%) in amino acid sequence between CYP2D4 and CYP2D6 whose structure has been resolved by X-ray crystallography [15]. We thus speculated that interactions between substrates and amino acid residues in the active-site cavity of CYP2D4 are complicated.

We previously found that the substitution of Phe-120 by alanine remarkably increased the capacity of CYP2D6 as a bunitrolol (BTL) 4-hydroxylase [13,14]. In that case, we considered that BTL is captured by Phe-120 of CYP2D6 via hydrophobic interaction (π–π interaction) between the aromatic rings of BTL and Phe-120, lowering the efficacy of the oxidation by interfering with the approach to the heme iron of another substrate molecule coming into the active-site cavity. On the basis of the inference and findings described above, we speculated that not multiple cavities to dock substrates but complicated interactions between the substrates and amino acid residues in the active-site cavity cause the non-Michaelis–Menten kinetics. In this study, we thus searched for possible roles of phenylalanine residues that can interact with BF and DEX in the active-site cavities of rat and human CYP2D isoenzymes.

We selected CYP2D4 as the frame in which to carry out the substitutions of amino acid residues. As candidates for amino acid residues of rat CYP2D4 to be substituted, we chose positions 109, 123, 216 and 486. That is, all of the CYP enzymes employed in the present study have one or more phenylalanine residue at these positions whose aromatic rings protrude into the active-site cavity. Wild-type CYP2D4 has Phe-109, Val-123, Leu-216 and Ala-486. Human CYP2D6 has phenylalanine residues at positions 120 and 483, corresponding to positions 123 and 486, respectively, of CYP2D4. CYP2D2 has Phe-216, and both CYP2D1 and CYP2D3 have Phe-486 (see Fig. 4). Furthermore, we recently found the importance of Phe-216 in the oxidation by rat CYP2D2 of 5-methoxy-*N*,*N*-diisopropyltryptamine (Foxy), a drug that can be abused [6]. Finally, we decided to substitute Phe-109 of CYP2D4 by isoleucine, an amino acid residue common to the other four CYP2D enzymes employed in this study, and the amino acid residues at positions 123, 216 and 486 of CYP2D4 by phenylalanine.

BF 1″-hydroxylation by wild-type CYP2D4 gave hook-shaped Eadie–Hofstee plots. Interestingly, the substitution of Val-123 or Ala-486 by phenylalanine changed the Eadie–Hofstee plots from hook-shaped to linear. Additionally, the

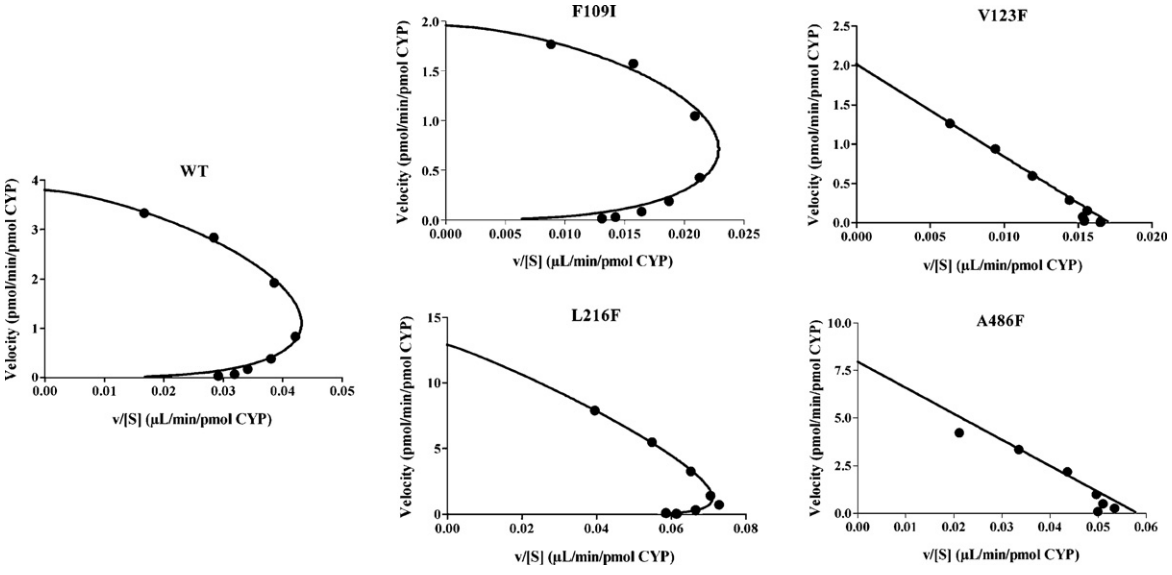

Fig. 5 – Eadie–Hofstee plots for BF 1″-hydroxylation by recombinant rat wild-type CYP2D4 and its four mutants. The substrate concentrations used were 2–500 μM. Typical plots from three determinations are shown.

Table 4 – Kinetic parameters for BF 1″-hydroxylation by microsomes from yeast cells expressing rat wild-type CYP2D4 and its mutants.

rCYP2D4	K_m or S_{50}[a]	V_{max}[b]	n[c]	CL_{int} or CL_{max}[d]
Wild-type[f]	49.2 ± 1.03**	3.69 ± 1.10	1.39 ± 0.032	0.041 ± 0.011
F109I[f]	46.2 ± 1.77	1.95 ± 0.20	1.55 ± 0.019	0.022 ± 0.003
V123F[e]	104 ± 28.9**	2.33 ± 0.43		0.023 ± 0.007
L216F[f]	108 ± 22.9**	8.64 ± 3.80*	1.17 ± 0.064**	0.053 ± 0.016
A486F[e]	91.3 ± 10.6*	4.76 ± 1.49		0.051 ± 0.012

Each value represents the mean ± S.D. for three separate experiments with independent preparations. rCYP, rat CYP.
[a] μM.
[b] pmol/min/pmol CYP.
[c] Hill coefficient.
[d] μL/min/pmol CYP.
[e] K_m, V_{max} and CL_{int} values were calculated by nonlinear regression to the Michaelis–Menten equation.
[f] S_{50}, V_{max} and CL_{max} values were calculated with the Hill equation.
* Significantly different from wild-type rCYP2D4 ($p < 0.05$).
** Significantly different from rCYP2D4 wild-type ($p < 0.01$).

substitution of Leu-216 by phenylalanine also tended to make the plots linear. DEX *O*-demethylation by wild-type CYP2D4 also exhibited hook-shaped Eadie–Hofstee plots. In contrast to the results for BF oxidation, only the substitution of Ala-486 with phenylalanine yielded linear Eadie–Hofstee plots for DEX *O*-demethylation with the substitution of neither Val-123 nor Leu-216 by phenylalanine changing the kinetic profile.

In the active-site cavity of human CYP2D6, substrates are thought to interact with Glu-216, Asp-301 and Phe-483 [15,17]. In the cases of CYP2D1 and CYP2D3, BF and DEX can interact with Asp-304 and Phe-486 in a similar manner. In the active-site cavity of CYP2D2, BF and DEX may interact with Glu-219, Asp-304 and Phe-216 instead of Ala-486. CYP2D4 has Leu-216, Asp-304 and Ala-486 so only CYP2D4 among the four rat CYP2D isoenzymes examined in this study does not have a phenylalanine residue that can interact with substrates at position 216, 304 or 486. We further identified Phe-109 of CYP2D4 as another candidate for hydrophobic (π–π) interaction with substrates.

The replacement of Phe-109 with isoleucine, a residue common to the other four enzymes (Fig. 4), did not have any effect on the kinetics of BF or DEX oxidation, indicating that Phe-109 of CYP2D4 is not involved in the interaction with these substrates. In the active-site cavity of CYP2D4, the basic nitrogen atom of the BF side-chain may ionically interact with the carboxylate group of Glu-219 or Asp-304, namely, in dual modes. The introduction of phenylalanine at position 486 causes hydrophobic (π–π) interaction with the aromatic ring of BF, which interferes with the ionic interaction of another BF molecule with the carboxylate group of Glu-219. This means that the modes of interaction in the active-site cavity of CYP2D4-A486F become simpler, resulting in linear kinetics.

It should be noted that K_m or S_{50} values for BF 1″-hydroxylation by CYP2D4-V123F, CYP2D4-L216F and CYP2D4-A486F increased by approximately two-fold as compared with the value for the wild-type enzyme, whereas the K_m value for DEX *O*-demethylation by CYP2D4-A486F was about one-half that of the corresponding S_{50} value for the wild-type CYP2D4. It is feasible that the mechanisms causing the alteration of kinetic profiles following the substitutions of amino acid residues by phenylalanine differ between BF 1″-hydroxylation and DEX *O*-demethylation, although a similar linearization was observed in Eadie–Hofstee plots.

The BF molecule has a slender shape, whereas the DEX molecule is bulky. BF with a basic nitrogen atom can be captured ionically by the carboxylate group of Glu-219 or Asp-304, resulting in an orientation whereby the oxidation site (1″-position) of the substrate comes close to the heme iron in dual modes. We speculated that the newly introduced phenylalanine at position 123 or 486 (also 216 at least in part) is involved in hydrophobic (π–π) interaction with the BF molecule. The substrate captured hydrophobically is not oxidized, but interferes with the interaction of another substrate with the carboxylate group of Glu-219 or Asp-304 in one of the dual modes described above. This might make the hook-shaped Eadie–Hofstee plots linear.

The DEX molecule can also be captured ionically with the carboxylate group of Glu-219 or Asp-304. Different from the results of BF 1″-hydroxylation, only the substitution of Ala-486 by phenylalanine caused the linear Eadie–Hofstee plots for DEX *O*-demethylation. As a possible explanation, the DEX molecule is trapped between the carboxylate group of Glu-219 (via ionic interaction with the basic nitrogen atom of DEX) and the phenyl group of Phe-486 (via hydrophobic interaction with the morphinan ring), resulting in an orientation whereby the methoxyl group of the substrate approaches the heme iron (Fig. 7). In this case, the introduction of phenylalanine at position 486 helps docking of the substrate into the active-site cavity, making the reaction modes simpler.

Rat CYP2D4 yielded hook-shaped Eadie–Hofstee plots for BF 1″-hydroxylation, whereas human CYP2D6 gave linear plots. The difference may be due to the phenylalanine residues of human CYP2D6 at positions 120 and 483, both of which can hydrophobically interact with BF and DEX in the active-site cavity. Rat CYP2D1 and CYP2D3 both have Phe-486 corresponding to position 483 of CYP2D6, and CYP2D2 has Phe-216 which seems likely to capture substrates. CYP2D4 has no phenylalanine residue at position 123, 216 or 486, instead, it has Phe-109. However, it is reasonable to think from the present results that Phe-109 is not involved extensively in the interaction with substrates. That is, CYP2D4 does not have the appropriate phenylalanine residues which can trap a substrate in the active-site cavity, causing hook-shaped kinetics. Further studies will be necessary to confirm this speculation.

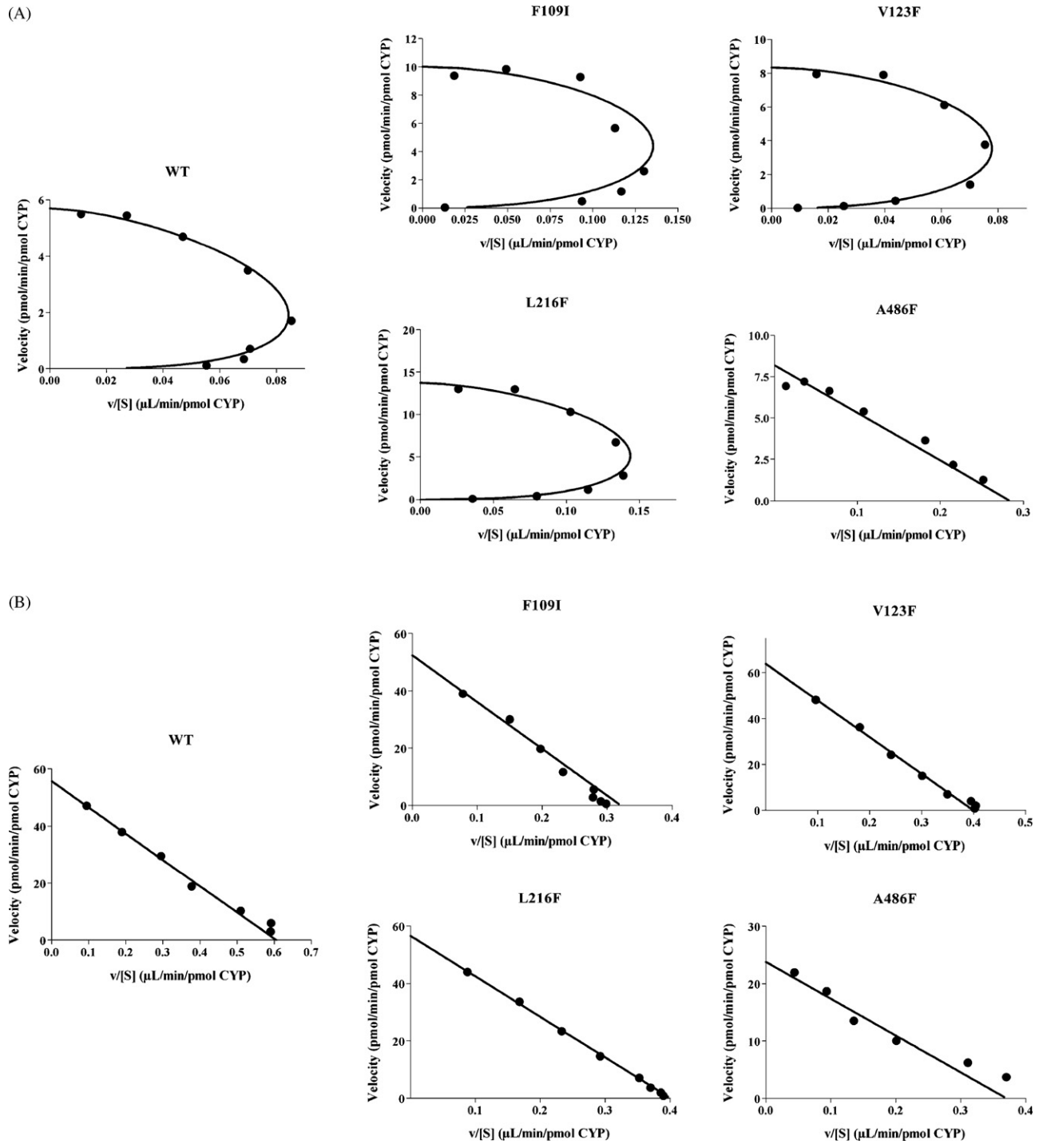

Fig. 6 – Eadie–Hofstee plots for DEX *O*-demethylation (A) and *N*-demethylation (B) by recombinant rat wild-type CYP2D4 and its four mutants. The substrate concentrations used were 2–500 μM. Typical plots from three determinations are shown.

In summary, the capacity to oxidize BF and DEX was compared kinetically between human CYP2D6 and four rat CYP2D enzymes in a yeast cell expression system. In BF 1″-hydroxylation and DEX *O*-demethylation, only CYP2D4 showed hook-shaped Eadie–Hofstee plots, the other four CYP2D enzymes exhibiting linear plots. In DEX *N*-demethylation, rat CYP2D2 did not show any detectable activity under the conditions used, while the other four enzymes yielded linear Eadie–Hofstee plots. Among four CYP2D4 mutants, CYP2D4-V123F, -L216F and -A486F yielded linear or linear-like Eadie–Hofstee plots in BF 1″-hydroxylation, whereas only CYP2D4-A486F exhibited linear plots in DEX *O*-demethylation. These results suggest that the introduction of phenylalanine into the active-site cavity of CYP2D4 simplifies the complicated interactions between the substrates and amino acid residues, but the mechanisms causing the simplification differ between BF and DEX.

Table 5 – Kinetic parameters for DEX oxidation by microsomes from yeast cells expressing rat wild-type CYP2D4 and its mutants.

rCYP2D4	K_m or S_{50}[a]	V_{max}[b]	n[c]	CL_{int} or CL_{max}[d]
O-Demethylation				
Wild-type[f]	43.2 ± 7.56	5.62 ± 0.25	1.43 ± 0.06	0.07 ± 0.01
F109I[f]	50.1 ± 13.7	9.64 ± 1.39	1.37 ± 0.22	0.12 ± 0.02
V123F[f]	63.5 ± 11.2**	9.92 ± 3.33*	1.48 ± 0.29	0.09 ± 0.03
L216F[f]	62.6 ± 12.8	13.9 ± 3.15**	1.34 ± 0.22	0.13 ± 0.03
A486F[e]	23.1 ± 0.78*	6.68 ± 1.79		0.29 ± 0.07**
N-Demethylation				
Wild-type[e]	94.6 ± 22.1	55.6 ± 0.65		0.61 ± 0.15
F109I[e]	143 ± 17.9	62.8 ± 13.4		0.45 ± 0.15
V123F[e]	202 ± 55.4*	33.2 ± 5.44		0.18 ± 0.07**
L216F[e]	150 ± 9.20	60.2 ± 22.8		0.40 ± 0.16
A486F[e]	81.6 ± 11.1	24.0 ± 3.17*		0.30 ± 0.07*

Each value represents the mean ± S.D. for three separate experiments with independent preparations. rCYP, rat CYP.
[a] μM.
[b] pmol/min/pmol CYP.
[c] Hill coefficient.
[d] μL/min/pmol CYP.
[e] K_m, V_{max} and CL_{int} values were calculated by nonlinear regression to the Michaelis–Menten equation.
[f] S_{50}, V_{max} and CL_{max} values were calculated with the Hill equation.
* Significantly different from wild-type rCYP2D4 ($p < 0.05$).
** Significantly different from wild-type rCYP2D4 ($p < 0.01$).

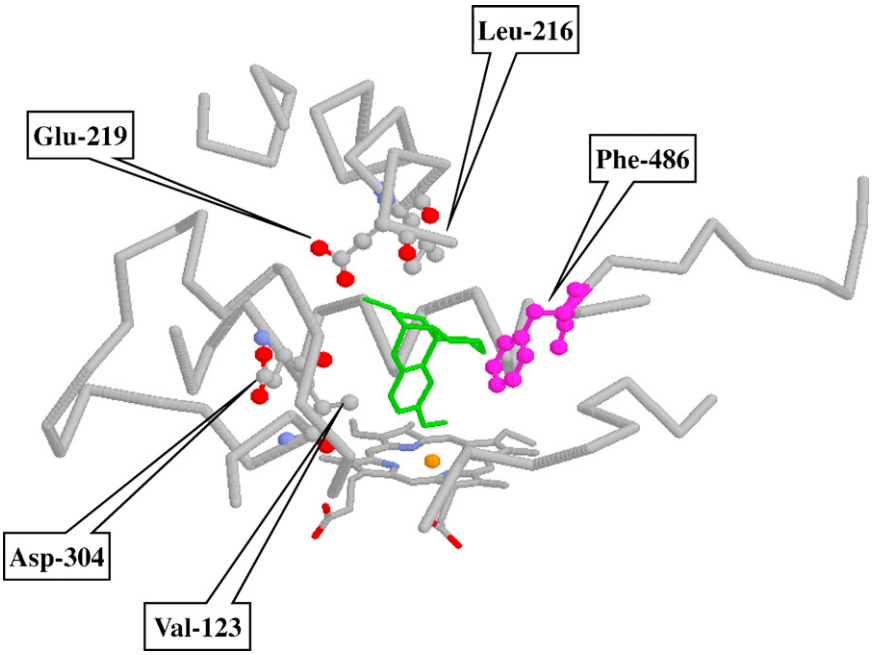

Fig. 7 – Interaction between DEX and amino acid residues in the active-site cavity of rat CYP2D4-A486F model. The conformation of the rat enzyme was constructed using the crystallographic data of CYP2D6 (2F9Q) as a template. The interaction mode was drawn with RasMol version 2.6-ucb-1.0. Amino acid residues at positions 123, 216, 219, 304 and 486 in ball-and-stick form, and DEX is in stick form. Hydrogen atoms of the amino acid residues and the substrate were omitted.

Acknowledgements

This work was supported in part by a Grant-in-Aid for Scientific Research (17390035) from the ministry of Education, Culture, Sports, Science and Technology of Japan.

REFERENCES

[1] Rendic S, Di Carlo FJ. Human cytochrome P450 enzymes: a status report summarizing their reactions, substrates, inducers and inhibitors. Drug Metab Rev 1997;29:413–580.

[2] Zanger UM, Raimundo S, Eichelbaum M. Cytochrome P450 2D6: overview and update on pharmacology, genetics, biochemistry. Naunyn-Schmiederberg's Arch Pharmacol 2004;369:23–37.
[3] Shimada T, Yamazaki H, Mimura M, Inui Y, Guengerich FP. Interindividual variations in human liver cytochrome P-450 enzymes involved in the oxidation of drugs, carcinogens and toxic chemicals: studies with liver microsomes of 30 Japanese and 30 Caucasians. J Pharmacol Exp Ther 1994;270:414–23.
[4] Evans WE, Relling MV. Pharmacogenomics: translating functional genomics into rational therapeutics. Science 1999;286:487–91.
[5] Ingelman-Sundberg M. Pharmacogenetics of cytochrome P450 and its applications in drug therapy: the past, present and future. Trends Pharmacol Sci 2004;25:193–200.
[6] Narimatsu S, Kiryu K, Yonemoto R, Yoshino M, Kobatake M, Kazamori D, et al. The roles of amino acid residues at positions 216 and 219 in the structural stability and metabolic functions of rat cytochrome P450 2D1 and 2D2. Chem Biol Interact 2008;172:11–21.
[7] Hiroi T, Imaoka S, Chow T, Funae Y. Tissue distributions of CYP2D1, 2D2, 2D3 and 2D4 mRNA in rats detected by RT-PCR. Biochim Biophys Acta 1998;1380:305–12.
[8] Niwa T, Okada K, Hiroi T, Imaoka S, Narimatsu S, Funae Y. Effect of psychotropic drugs on the 21-hydroxylation of neurosteroids, progesterone and allopregnanolone, catalyzed by rat CYP2D4 and human CYP2D6 in the brain. Biol Pharm Bull 2008;31:348–51.
[9] Kishimoto W, Hiroi T, Shiraishi M, Osada M, Imaoka S, Kominami S, et al. Cytochrome P450 2D catalyze steroid 21-hydroxylation in the brain. Endocrinology 2004;145:699–705.
[10] Suzuki T, Narimatsu S, Fujita S, Masubuchi Y, Umeda S, Imaoka S, et al. Purification and characterization of a cytochrome P-450 isozyme catalyzing bunitrolol 4-hydroxylation in liver microsomes of male rats. Drug Metab Dispos 1992;20:367–73.
[11] Masubuchi Y, Kagimoto N, Narimatsu S, Fujita S, Suzuki T. Regioselective contribution of the cytochrome P-450 2D subfamily to propranolol metabolism in rat liver microsomes. Drug Metab Dispos 1993;21:1012–6.
[12] Masubuchi Y, Hosokawa S, Horie T, Ohmori S, Kitada M, Suzuki M, et al. Cytochrome P-450 isozymes involved in propranolol metabolism in human liver microsomes: the role of CYP2D6 as ring-hydroxylase and CYP1A2 as *N*-desisopropyrase. Drug Metab Dispos 1994;22:909–15.
[13] Masuda K, Tamagake K, Okuda Y, Torigoe F, Tsuzuki D, Isobe T, et al. Change in enantioselectivity in bufuralol 1″-hydroxylation by the substitution of phenylalanine-120 by alanine in cytochrome P450 2D6. Chirality 2005;17:37–43.
[14] Masuda K, Tamagake K, Katsu T, Torigoe F, Saito K, Hanioka N, et al. The roles of phenylalanine at position 120 and glutamic acid at position 222 in the oxidation of chiral substrates by cytochrome P450 2D6. Chirality 2006;18:167–76.
[15] Rowland P, Blaney1 FE, Smyth MG, Jones JJ, Leydon VR, Oxbrow AK, et al. Crystal structure of human cytochrome P450 2D6. J Biol Chem 2006;281:7614–22.
[16] Guengerich FP, Hanna IH, Martin MV, Gillam EM. Role of glutamic acid 216 in cytochrome P450 2D6 substrate binding and catalysis. Biochemistry 2003;42:1245–53.
[17] Paine MJ, McLaughlin LA, Flanagan JU, Kemp CA, Sutcliffe MJ, Roberts GC, et al. Residues glutamate 216 and aspartate 301 are key determinants of substrate specificity and product regioselectivity in cytochrome P450 2D6. J Biol Chem 2003;278:4021–7.
[18] Ellis SW, Hayhurst GP, Smith G, Lightfoot T, Wong MM, Simula AP, et al. Evidence that aspartic acid 301 is a critical substrate-contact residue in the active site of cytochrome P450 2D6. J Biol Chem 1995;270:29055–8.
[19] Gotoh O. Substrate recognition sites in cytochrome P450 subfamily 2 (CYP2) proteins inferred from comparative analyses of amino acid and coding nucleotide sequences. J Biol Chem 1992;267:83–90.
[20] Tsuzuki D, Takemi C, Yamamoto S, Tamagake K, Imaoka S, Funae Y, et al. Functional evaluation of cytochrome P450 2D6 with Gly42Arg substitution expressed in *Saccharomyces cerevisiae*. Pharmacogenetics 2001;11:709–18.
[21] Wan J, Imaoka S, Chow T, Hiroi T, Yabusaki Y, Funae Y. Expression of four rat CYP2D isoforms in *Saccharomyces cerevisiae* and their catalytic specificity. Arch Biochem Biophys 1997;348:383–90.
[22] Narimatsu S, Imoto K, Isobe T, Kiryu K, Naito S, Hichiya H, et al. The roles of amino acid residues at positions 43 and 45 in microsomal contents and enzymatic functions of rat CYP2D1 and CYP2D2. Biochem Biophys Res Commun 2004;324:627–33.
[23] Hichiya H, Takemi C, Tsuzuki D, Yamamoto S, Asaoka K, Suzuki S, et al. Complementary DNA cloning and characterization of cytochrome P450 2D29 from Japanese monkey liver. Biochem Pharmacol 2002;64:1101–10.
[24] Guengerich FP, Wang P, Davidson NK. Estimation of isozymes of microsomal cytochrome P-450 in rats, rabbits, and humans using immunochemical staining coupled with sodium dodecyl sulfate-polyacrylamide gel electrophoresis. Biochemistry 1982;21:1698–706.
[25] Omura T, Sato R. The carbon monoxide-binding pigment of liver microsomes. I. Evidence for its hemoprotein nature. J Biol Chem 1964;239:2370–8.
[26] Hanioka N, Okumura Y, Saito Y, Hichiya H, Soyama A, Saito K, et al. Catalytic roles of CYP2D6.10 and CYP2D6.36 enzymes in mexiletine metabolism: *in vitro* functional analysis of recombinant proteins expressed in *Saccharomyces cerevisiae*. Biochem Pharmacol 2006;71:1386–95.
[27] Kronbach T, Mathys D, Gut J, Catin T, Meyer UA. High-performance liquid chromatographic assays for bufuralol 1′-hydroxylase, debrisoquine 4-hydroxylase, and dextromethorphan O-demethylase in microsomes and purified cytochrome P-450 isozymes of human liver. Anal Biochem 1987;162:24–32.
[28] Williams PA, Cosme J, Vinkovic DM, Ward A, Angove HC, Day PJ, et al. Crystal structures of human cytochrome P450 3A4 bound to metyrapone and progesterone. Science 2004;305:683–6.